# Status of SPIDER beam source after the first 3.5 years of operation

M. Pavei[a], C. Gasparrini[a,b,†*], G. Berton[a], M. Agostini[a,c], V. Candela[d], V. Candeloro[a,d], C. Cavallini[a,d], M. Dan[a], S. Denizeau[a], M. Fadone[a], B. Pouradier Duteil[a,e], A. La Rosa[a], N. Marconato[a], B. Segalini[a,d], M. Spolaore[a,c],S. Deambrosis[f], E. Miorin[f], F. Montagner[f], D. Badocco[g], P. Pastore[g], R. Nocentini[h], S. Dal Bello[a], L. Grando[a,c], M. Boldrin[a], D. Marcuzzi[a], A. Rizzolo[a], E. Sartori[a,d], P. Sonato[a,d], G. Serianni[a,c]

[a] Consorzio RFX (CNR, ENEA, INFN, UNIPD, Acciaierie Venete SpA), Corso Stati Uniti 4 – 35127 Padova, Italy
[b] Department of Materials & Centre for Nuclear Engineering, Imperial College London, SW7 2AZ, London, UK
[c] ISTP-CNR, Institute for Plasma Science and Technology, Italy
[d] Padua University, via VIII Febbraio 2, 35122 Padova, Italy
[e] Swiss Plasma Center (SPC), Ecole Polytechnique Fédérale de Lausanne (EPFL), CH-1015 Lausanne, Switzerland
[f] Institute of Condensed Matter Chemistry and Technologies for Energy, National Research Council of Italy (ICMATE-CNR), Corso Stati Uniti 4 – 35127 Padova, Italy
[g] Department of Chemical Sciences, Padua University, Via Marzolo 1, 35131, Padova, Italy
[h] Max-Planck-Institut für Plasmaphysik, Boltzmannstr. 2, 85748 Garching, Germany

[†] RINA S.p.A, Italy
**Keywords:** neutral beam injectors – materials degradation – caesium – particles interaction - coating

**Abstract**

SPIDER is the negative ion source testbed for ITER neutral beam injector. It is currently the largest negative ion source ever built, equipped with a 100 keV accelerator, aiming at producing a negative ion beam with an extracted current density in hydrogen of 355 A/m$^2$, beam-on time of one hour. During the first 3.5 years of operation several improvements on the SPIDER source and its operating conditions were implemented. This paper focuses on the description of materials degradation phenomena in SPIDER and on the lessons learnt that were derived from components inspection during the already planned shutdown in 2022. The aim of these inspections was to improve the design of some components and to repair or refurbish damaged components. In particular, this paper describes the characterisation of damaged molybdenum coating, testing of surface cleaning techniques and experimental evidence of caesium vapour uneven distribution inside the plasma chamber. Sputtering due to beam particles was also investigated experimentally to observe its effect on materials used in SPIDER.

## 1. Introduction

A combination of additional heating and current drive systems is necessary for ITER to reach fusion conditions and to control plasma configuration. Among them, two Neutral Beam Injectors (NBI) will provide 33MW hydrogen/deuterium particles, electrostatically accelerated to 1 MeV.

To reach efficient neutralisation at such beam energy, the use of negative ions is required by conversion of atoms and positive ions thanks to the interaction with caesiated surfaces. NBI requirements have never been simultaneously attained; hence, the ITER Neutral Beam Test Facility (NBTF) was built at Consorzio RFX (Italy). Its aim is to prove that these requirements can be obtained in the MITICA experiment, the full-scale NBI prototype with 1MeV particle energy. SPIDER, a 100keV particle energy source, is devoted to test and optimise the full-scale ion source requirements reaching the goals of: extracted beam uniformity, negative ion extracted current density (355/285 A/$m^2$ in hydrogen/deuterium for 3600s) and beam optics[1].

SPIDER started operation in June 2018. The experimental programme involved some years without caesium[2]. In 2021, caesium was injected for the first time and higher current density beams were extracted and accelerated[3]. The operating conditions with Cs injection were up to 50kW per driver, with pulses duration between 15-30 seconds reaching negative ion current of approximately 160 A/$m^2$ at the extraction, with an acceleration energy below 50 keV[[4]].Soon after, a shutdown scheduled for 2021 was started for the improvement of several components of the beam source, in particular: the on-board Radio-Frequency (RF) matching circuit [5], RF power supplies (replacing the tetrode-based RF generators with solid-state amplifiers),, pumping system and vacuum quality (with the installation of non-evaporable getter, NEG, pumps[6]) and beam source refurbishment. the on-board Radio-Frequency (RF) matching circuit[5] , RF power supplies (replacing the tetrode-based RF generators with solid-state amplifiers), pumping system and vacuum quality (with the installation of non-evaporable getter, NEG, pumps[6]), beam source refurbishment. During the shutdown, the beam source was completely taken out of the vacuum vessel, dismantled and characterised. The structure of the beam source can be seen in Figure 1. Dismantling the beam source allowed the inspection of the plasma-facing components for the first time after the first three and a half years of operation. Unforeseen damages were detected by visually inspecting the components; hence an experimental campaign supported by modelling efforts began to better understand the materials degradation phenomena observed in SPIDER beam source. The modelling and experimental study conducted highlighted the evidence of: non-uniform distribution of caesium across the plasma chamber; back-streaming positive ions (BSI) impinging on the rear side of the plasma box and removing the caesium layer; interaction of plasma with surfaces. Electrical discharges outside and inside the source, which had already been observed, were confirmed. The relationship between beam and source non-uniformity was previously related to local profiles of plasma features, plasma expansion out of the RF drivers, a possiblenon-uniformity of caesium distribution over the PG[7]. It was found that generation of negative ions was enhanced by increasing the caesium injection rate[7].

In this work we found experimental evidence of caesium non-uniformity inside SPIDER beam source components. This was possible using experimental techniques conducted on disassembled components that were inevitably exposed to air atmosphere during the shutdown and modelling techniques.

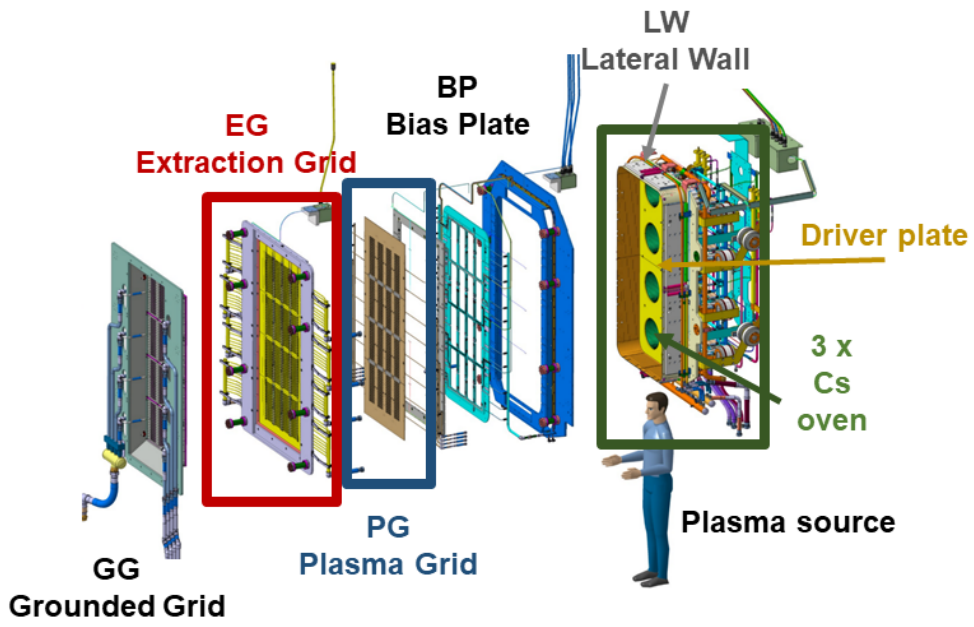


Figure 1 Schematic of the main components of the SPIDER beam source; highlighted are the main components that were investigated in the present work: extraction grid, plasma grid, lateral wall and driver plate (the side of the driver exposed to the plasma is dubbed Plasma Driver Plate – PDP).

Inspections showed that the molybdenum coating deposited on all plasma-facing SPIDER beam source components was damaged; coating characterisation was therefore performed to better understand how it got damaged and how to improve it for the future. A method for removing the previously damaged molybdenum coating and coating redeposition was preliminarily tested in collaboration with industries and laboratories involved in the development of the main components of the negative ion beam source. To study caesium distribution across the source components, modelling was accompanied by sampling and chemical characterisation. Caesium distribution was quantified by Inductively Coupled Plasma Mass Spectrometry (ICP-MS) across the Lateral wall and on the Plasma Driver Plate highlighting the dual effect of ballistic Cs distribution (from Cs oven nozzles) and plasma redistribution effect. Analyses on the extraction grid were performed since some unexpected stains were observed. Evidence of copper sputtering due to beam particles interaction on extraction grid apertures highlighted the need for their refurbishment to increase the beam clearance, this had been planned according to model predictions. Components damaged due to accidents (such as water leaks) were observed and their repair was necessarily carried out during the major shutdown.

## 2. Material and methods

### Sampling – chemical analysis on caesium

Chemical analysis on SPIDER surfaces was performed using swab sampling and analysis with ICP-MS. The method involved the use of a nitric acid solution made with ultrapure water (UPW)[8] as a solvent. UPW was produced in-house at Consorzio RFX[9], it was additivated with a reagent grade 67-69% nitric acid of high purity quality to limit any metal cross contamination from the nitric acid[10][11]. 2 g of 5% $HNO_3$ was used as sampling solution. A cotton swab submerged in

the nitric acid was stirred for approximately 30 seconds and then thoroughly squeezed. Stains from SPIDER Beam source components were sampled using the swab by applying a circular motion on the area of interest (applying a soft pressure for approximately 5 seconds), the cotton swab was then submerged in the vial and stirred for 30 seconds. The weight of the solution was quantified and the area of interest sampled by the swab was photographed before and after sampling to measure the exposed surface area. The solution was analysed by ICP-MS for trace metal analysis using an ICP-MS Agilent Technologies 7700x system. Data obtained from the swabs taken on the Plasma Grid (PG) were plotted upon normalizing Cs with Cu quantified in the solution. Data obtained from the swabs taken on the PDP across BSI footprints were plotted without normalisation.

**Characterisation of surfaces**

Solid corrosion products found in SPIDER Beam Source were characterised in secondary electron and backscattered mode using a scanning electron microscope (SEM) and analyzed with energy dispersive X-ray spectroscopy (EDX). An ESEM FEI Quanta 200 equipped with EDX analysis was used in collaboration with Centro di Analisi e Servizi Per la Certificazione (CEASC), Padua, Italy and a FE-SEM Sigma Zeiss EDS Oxford X-MAX was used in collaboration with Institute of Condensed Matter Chemistry and Technologies for Energy, National Research Council of Italy, ICMATE-CNR.

## 3. Results and discussion

SPIDER beam source is subjected during operation to challenging phenomena such as: interaction with high energy beam particles, thermal and mechanical stresses and corrosion.

During the first 3.5 years of experimental campaign SPIDER negative ion current performance have improved thanks to the implementation of caesium-catalysed surfaces, but inevitably the operation of this complex machine had to withstand unforeseen circumstances like accidents and materials degradation. The long shutdown planned for the improvement of the vacuum system, RF drivers and circuits on board the beam source and RF generators has been exploited for the improvement of SPIDER components damaged during operation and to study the effect of the beam particles interacting with SPIDER source components and materials degradation during operation. Notably, at the opening of SPIDER beam source, many components were found damaged and degraded, see Figure 2 .

**Molybdenum coating**

Figure 2 shows photos of the PG, a close-up of PG apertures and a photo of the Plasma Driver Plate (PDP). These components were originally molybdenum coated to enable operation with caesium. Molybdenum coating was chosen to protect copper from the effect of impinging high energy beam particles and to maximise the formation of negative ions, since caesium deposited on top of molybdenum minimises its work function[12].

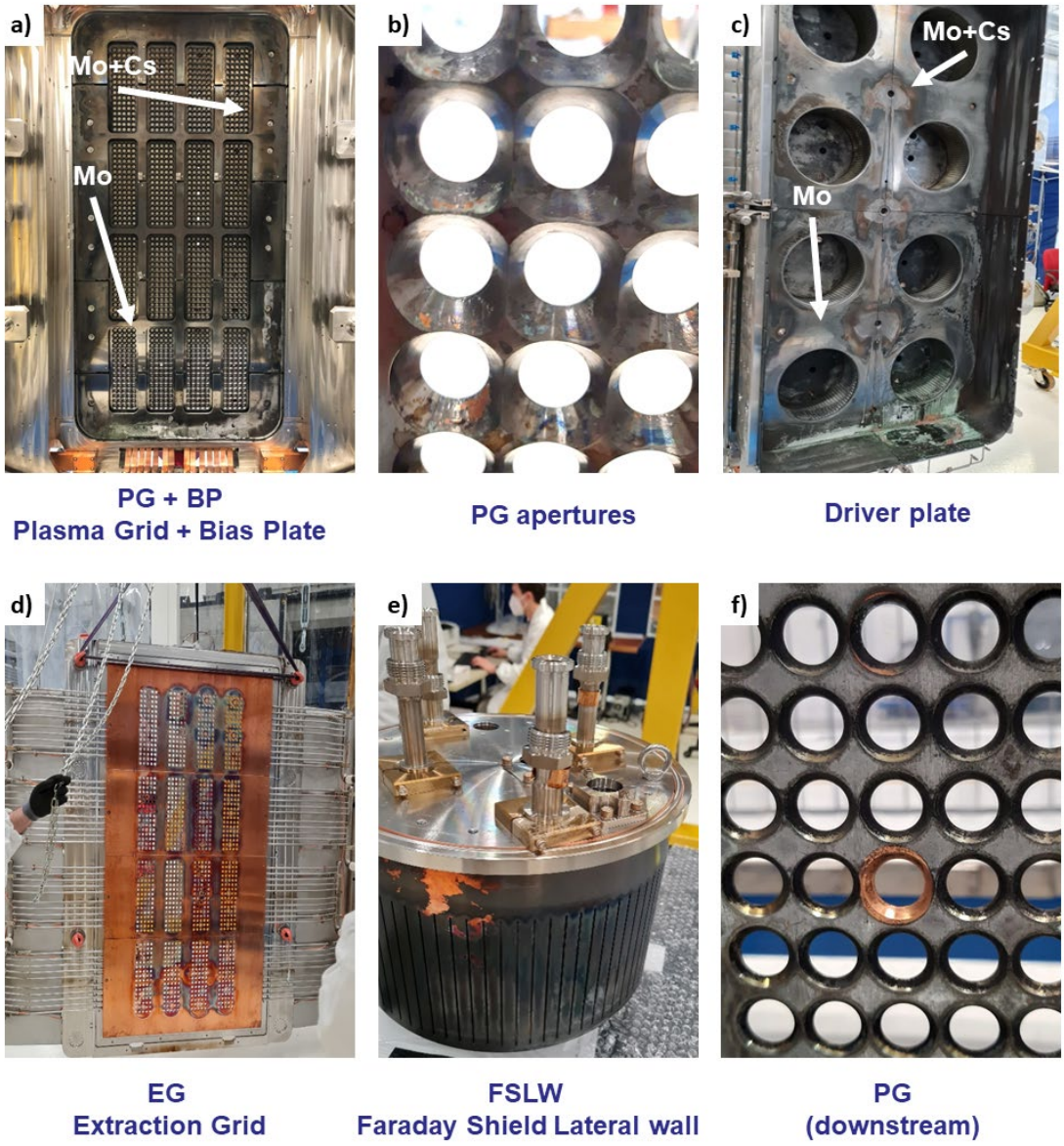


Figure 2 Photos from SPIDER beam source: a) Plasma grid and bias plate (upstream side) showing evidences of an accident (water leak at the bottom of the source), b) Plasma grid apertures with deflaked molybdenum coating, c) Plasma Driver Plate covered with caesium and showing evidences of BSI footprints, d) extraction grid (EG), e) Faraday shield lateral wall with the molybdenum coating damaged, f) plasma grid with copper redistribution (downstream side)

Molybdenum coating was found damaged, see PG aperture visual inspection in Figure 2b; molybdenum chips were found and characterised by SEM. SEM analysis was used to characterise the coating before and after operation in SPIDER to improve the manufacturing process in view of SPIDER beam source refurbishment and restart planned for 2023. Figure 3a shows secondary electron images (SEIs) of top surface and cross section of SPIDER-like coatings (samples courtesy of IPP Garching - Max Planck Institute for Plasma Physics that commissioned the coating). This coating was commissioned by IPP for NNBI testbeds in Garching, Germany, and has been labelled SPIDER-like because this coating was manufactured with the same process, by the same company and in the same year as SPIDER beam source components. The morphology of SPIDER-like Mo coating showed a columnar dendritic structure and a roughness Ra = 0.49µm. Figure 3a shows

SPIDER coating morphology after operation in the source for 3.5 years. SEM images of SPIDER coating were taken from SPIDER Faraday Shield Lateral Wall (FSLW) component which was found irremediably damaged from the water leak accident occurred in 2021 during operation. FSLW damaged component was sliced to obtain samples that could be used to test decoating procedures and characterisation of the coating for molybdenum refurbishment. A chemical decoating procedure was applied to half of the sample shown in Figure 3 to reveal the copper surface and the original coating. Figure 3b SEIs showed SPIDER coating after 3.5 years operation, the morphology was dendritic, similarly to Figure 3a. Cracks were observed on SPIDER coating (see Figure 3b), these may have been induced by thermal and mechanical shocks during operation. Figure 3c shows the morphology of a newly developed coating which did not present the dendritic columnar structure.

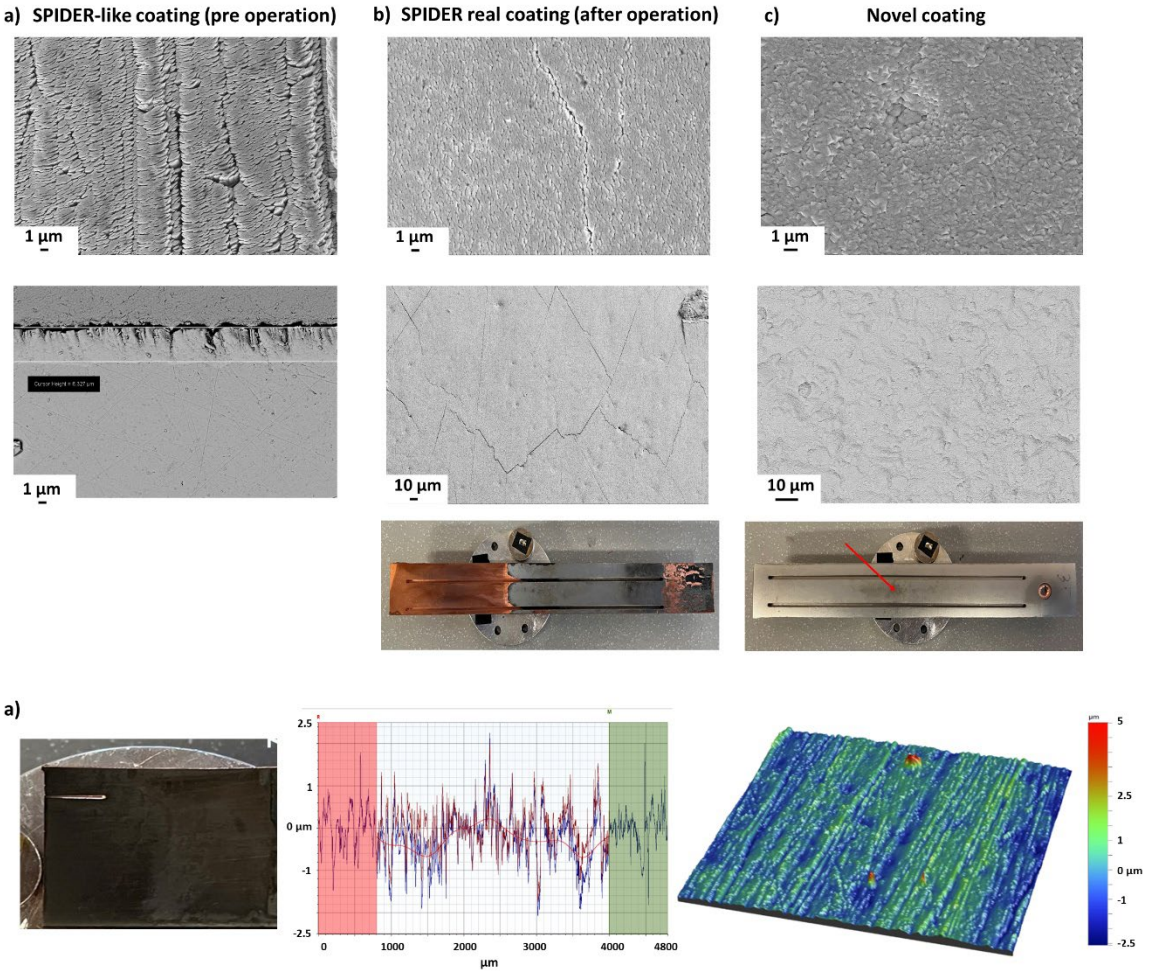


Figure 3 SE images (SEI) of molybdenum coating: a) SE images of SPIDER-like coating as manufactured: top surface and cross section, photo of the coupon and a rugosity and profilometry map (shown at the bottom); b) SPIDER coating top surface after 3.5 years of operation: SEM analyses were made on molybdenum coating that appeared not damaged, partial decoating of the sample was intentional to allow characterisation of the copper surface underneath, c) an example of a proposed molybdenum novel coating morphology - as manufactured

It should be noted that, depending on the orientation of the sample inside the deposition chamber used for the plasma vapour deposition (PVD) process to manufacture the molybdenum

coating, a dendritic or a non-dendritic morphology can be observed in SPIDER-like coatings, see Figure 4.

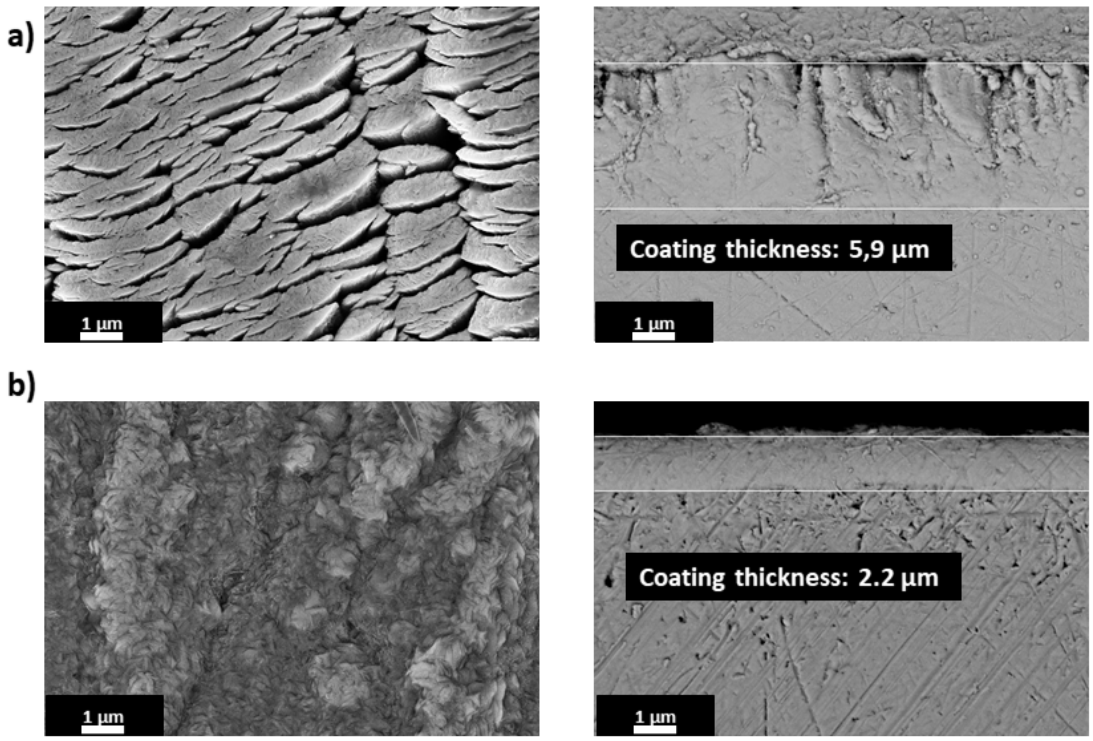


Figure 4 Top surface and cross section SEIs of SPIDER-like Mo coating on Cu samples exposed: a) normally to the Mo target showing a columnar morphology and b) vertically to the Mo target showing a non-columnar morphology

**Caesium evaporation**

All plasma-facing surfaces (i.e. source walls, driver Faraday Shield Lateral Walls, driver backplate, PG and BP) are molybdenum coated to prevent copper from sputtering into the source plasma and to maximise the effective operation of caesium. Caesium is evaporated in SPIDER beam source inside three ovens mounted in the rear of the beam source[13][14][15]. Caesium evaporation should enable a full and homogeneous caesium coverage over the PG to reduce local beamlet-to-beamlet differences in negative ion production. The caesium layer should be deposited in the order of few monolayers to maintain a constant work function (2.1 eV[12]). The opening of the source enabled the inspection of the components opposite the caesium ovens and the characterisation of caesium deposited layer. An optimised caesium conditioning of SPIDER PG is particularly important for the extraction of negative ions. Caesium distribution on the microscale on the PG cannot be considered homogeneous given the non-perfectly smooth molybdenum coating surfaces characterising the PG and other plasma facing components (see profilometry map in Figure 2).

Caesium rapidly reacts when is exposed to air; therefore, surface analyses aimed at caesium characterisation can only give a qualitative assessment since they were carried out in SPIDER beam source components after they were exposed to air for months. Additionally, due to a water leak, in some areas the caesium layer was completely altered with respect to the status during

operation, and visual inspection indicated a complete removal in some areas. To assess the caesium distribution across the PG, some preliminary analyses were conducted on some Langmuir probe electrodes made of molybdenum that were mounted on the Bias Plate (BP). SEM analysis revealed the presence of caesium using EDX mapping.

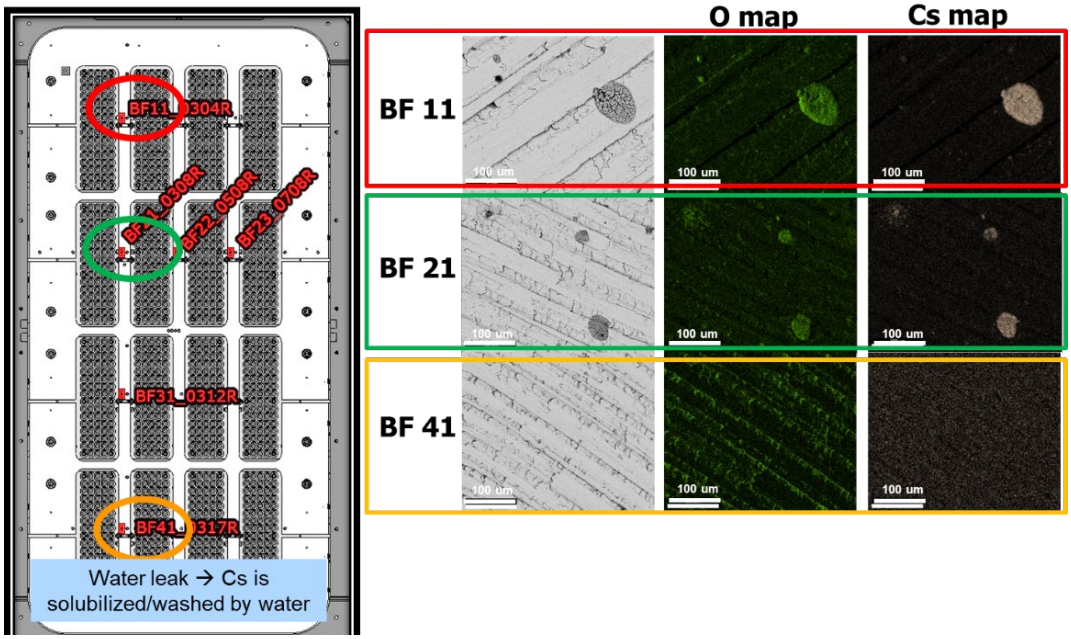


Figure 5 BP showing the position of probes used to monitor caesium distribution, SEIs on the molybdenum plates of Langmuir probes showing evidence of caesium in the form of stains

Figure 5 shows the BP and PG with the position of the Langmuir probe electrodes [16] that were removed to verify the caesium distribution. SEIs showed caesium distributed in the form of pits/stains. The analyses were made on the probes[17] after being exposed to the atmosphere and therefore this may not be representative of the caesium layer deposited under vacuum in SPIDER during operation. As discussed earlier, it was the bottom part of the source that was affected by the water leak, and the BP and PG were directly exposed: no caesium could be detected on the surface of the probes (see Figure 5). This confirms the effective role of ultrapure water in solubilising caesium.

Relative quantitative information on the amount of caesium present on SPIDER surfaces was obtained using chemical analyses. Samples were taken using a swab soaked in a 5% $HNO_3$ solution as described in the experimental section. A procedure was defined to control the collection area (tape with circular holes), and the duration of the swab application. In relative terms among the sampling swabs, a quantitative estimation could be carried out, and the amount of base material in the solution was used to correct the estimation. This methodology can be applied to any surface; however, in the following, this technique was used to study caesium evaporation and distribution without plasma. To track caesium distribution, sampling was performed on the EG surface on the side facing the plasma. Circular stains were visible, these were interpreted as the projection of the plasma grid aperture along straight lines pointing towards the three caesium ovens. For this reason, stains were associated to the flux of neutral caesium directly proceeding from the ovens and during the pause between plasma discharges; during the plasma discharge, a considerable fraction of caesium was transported towards the plasma grid in the form of positive ions that could not exit the source because of the applied extraction electrical field.

The nitric acid solution was capable of removing/cleaning the opaque layer that was labelled as "stain" in Figure 6b(left). The footprint left from swabbing the stain is shown in Figure 6b (right). The footprint was used to estimate the area sampled and normalise the ion concentration measured by ICP-MS with the total area swabbed. ICP-MS confirmed the presence of caesium in the stains found on the EG. The use of nitric acid enabled the removal of part of the copper surface as can be seen in the graph in Figure 6b (left) where the copper surface is revealed with a shiny appearance. The presence of caesium and copper in the area was accompanied by the presence of molybdenum, tungsten and rhenium. Sputtered molybdenum, removed by plasma interaction or by impact with backstreaming positive ions (BSI+), could be redeposited onto the EG surface, which instead is not molybdenum-coated. Tungsten and rhenium were used as alloy in the filaments of the RF drivers to start the plasma, hence the presence of these elements in the EG are associated with the degradation/consumption of the filaments during SPIDER operation.

Figure 6c shows a good agreement between experimental data and numerical simulations. Specifically, the red triangles are the experimental data, ratio between caesium and copper, from ICP-MS analysis on the swabs taken on the EG. Keeping in mind that the swab footprint, the area sampled, was as uniform as possible for all samples, the normalisation was performed considering the amount of copper analysed. AVOCADO software has been used for the numerical simulations. It is a code with which it is possible to study the pressure distribution of a gas and it takes into account only the gas particles-wall collisions with a cosine angle diffusion approach[18]. In this case, Figure 6a shows the caesium ovens arrangement and the line-integrated caesium density simulated at 1 cm from the PG considering ovens 3 & 2 evaporating at 0.7 [Pa·m/s] and oven 1 at 0.6 [Pa·m/s] (with a sticking factor of 60 %) and 28 apertures open. During SPIDER campaign with Cs, the extracted beam was found to be vertically non-uniform[3]. A vertical non-uniformity is also confirmed by the measurements of the Cs density by Laser Absorption Spectroscopy (LAS)[19]. In order to match these experimental evidences, the Cs flux for the bottom oven was set at a lower value than the other two ovens in the numerical simulations. The model does not have the EG geometry incorporated, but it can be used as a reference since the EG stains are caused by the caesium deposition during the plasma-off period: the different up and down position of the stains around the holes shows a direct dependence on the caesium oven position. The few discrepancies between the modelling and experimental data points may be related to several causes, possibly: the handling procedure of the EG during disassembly and prior to sampling, furthermore the circular stains were not all consistent since they possibly were affected by the impinging beam. The overall trend, though, is in line with the modelling results (see graph in Figure 6c).

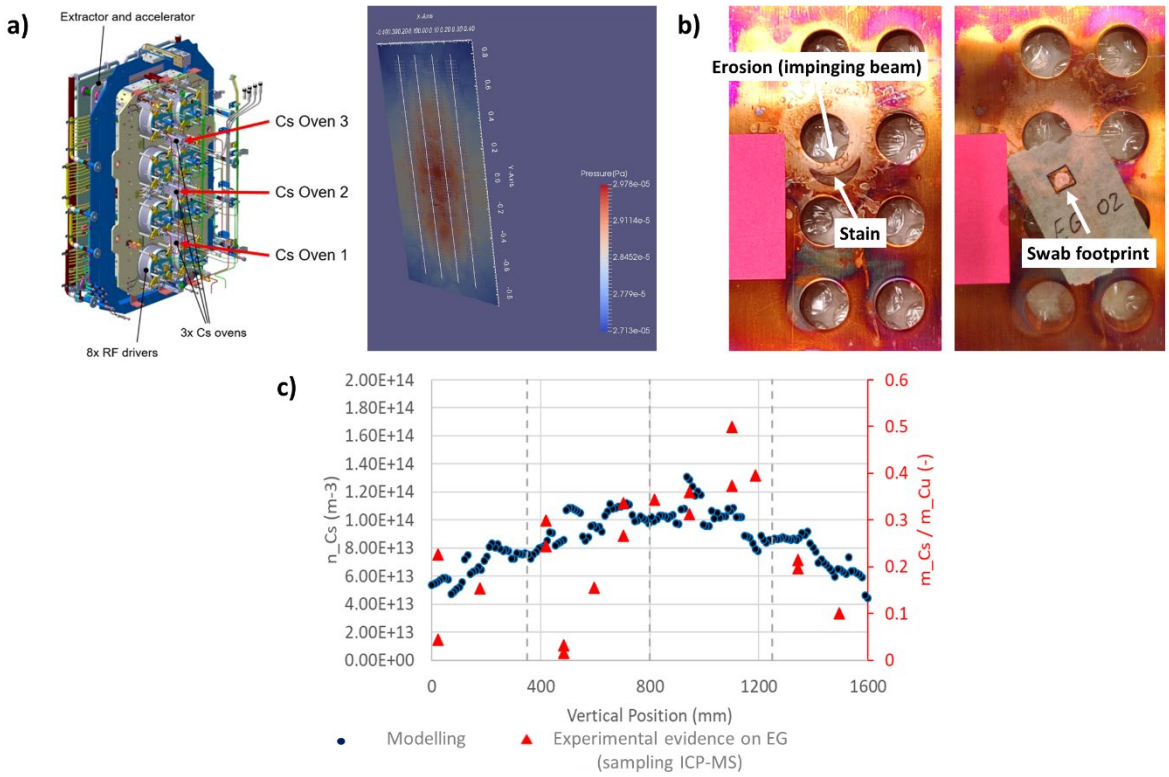


Figure 6 a) caesium oven distribution and caesium distribution on the PG from AVOCADO simulations, b) photos of the EG surface pre and post sampling showing the circular stains samples and the regions nearby eroded by the impinging beam, c) comparison between AVOCADO simulations and sampling on EG circular stains

Sampling for caesium detection was conducted also on SPIDER lateral wall to investigate the distribution of caesium during plasma operation. Lateral Wall (LW) surrounds the plasma chamber and its walls are subjected to plasma interaction. Stripes of different colours were visually observed on the LW and these were swabbed to understand the distribution of metallic elements; the results suggest that the plasma was capable of redepositing caesium (Figure 7). The magnetic field[20] generated by 4 arrays of permanent magnets (mounted behind the walls) drastically influenced the distribution of caesium. It was found that the LW plates intercepting the filter field lines perpendicularly exhibited a greater concentration of caesium in correspondence of the cusp magnets, where the plasma wall interaction is localised, and a lower amount in between. The opposite result was found at the upper LW, possibly indicating that the vertical plasma diffusion in the expansion region is impeded as it is perpendicular to the filter field, while it is facilitated along the parallel direction. During plasma operation, caesium is desorbed from the rear driver plate, where high concentration is found around the caesium ovens, then it is ionised and transported by the plasma to the lateral walls in the form of $Cs^+$. Modifications of the magnetic field to improve the plasma confinement in SPIDER are currently ongoing. The analyses of the Cs deposition on the LW helped us better understand how this new magnetic configuration could affect the Cs redistribution in the source.

Figure 7 Cs distribution on the LW, photos of the LW showing evidence of metallic deposition, Cs was quantified using ICP-MS across the coloured (brown-ish and grey-ish) stripes

**Caesium cleaning procedures**

SPIDER experimental campaign proved that the source may be exposed to air atmosphere for long periods during maintenance operation (more than a day). This can affect caesium layer deposited on the source walls. In perspective, it is necessary to assess the best way to remove caesium compounds during maintenance operations. Given the needs to evaporate caesium on a clean surface, some preliminary cleaning procedures were tested on SPIDER components. Cleaning procedures involved the use of: ultrapure water, acid (citric and nitric acid of several concentrations), $CO_2$ ice blasting and the execution of glow discharges in argon and helium (see Figure 8). Cleaning options were tailored to remove powder deposits (e.g. green copper oxides, or white deposits made of cesium hydroxide), dark stains and caesium shadows (caesium oxide)[17]. So far the efficacy of the adopted cleaning methods was evaluated by visual inspections or by SEM analysis highlighting the effective recovery of surface shininess using nitric or acid solutions and He glow discharge, however, the Cs efficient removal was yet to be demonstrated for all cleaning procedure tested.

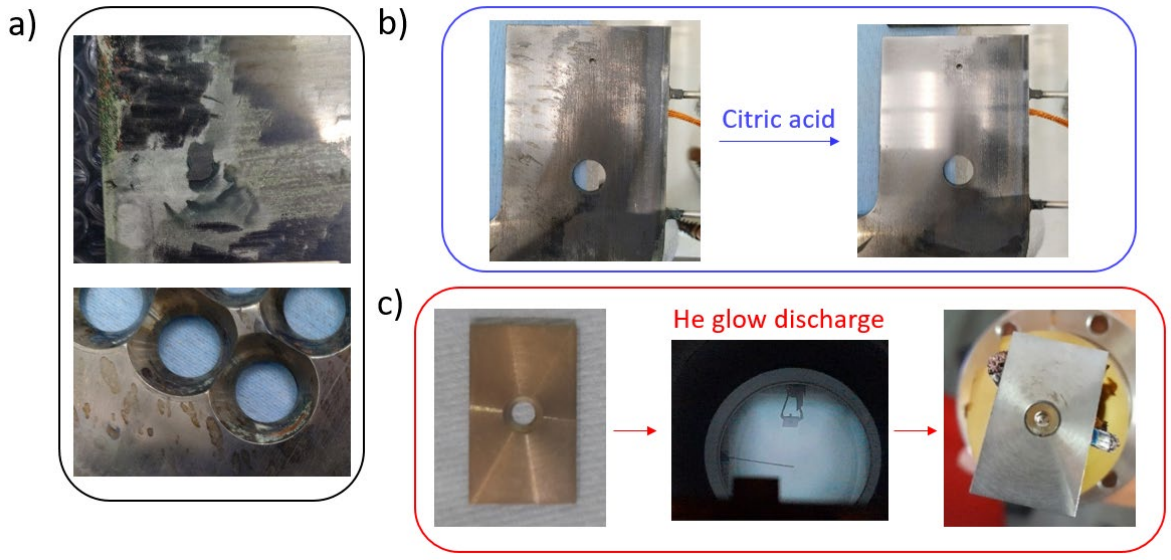


Figure 8 ) Examples of typical stains and shadows found in the source after operation, b) cleaning of a BP segment using a citric acid solution, c) cleaning of a probe installed on the BP by glow discharge in He

Cleaning techniques will be optimized in the future keeping in mind that cleaning of the ITER NBIs would have to be performed without disassembling the source and remotely. Tailored analysis on the effective removal capability of caesium will be performed in the future using chemical analyses to quantify caesium before and after each cleaning procedure in order to give definitive indications on the effective cleaning performance.

**Backstreaming positive ions**

It is known that backstreaming positive ions (BSI+) are produced in the accelerating column due to several phenomena, among which ionization of the background gas, double stripping during impact of beam negative ions with the background gas, or even sputtering of charges from the electrodes. These positive ions are then accelerated back inside the source with an energy depending on their birth position along the beam axis (the closer to the exit of the accelerator, the higher the energy), ultimately impacting on the rear surfaces of the source. BSI+ are commonly found in negative ion sources to contribute to caesium recycling from the rear surface of the ion source, and therefore to a better sustainment of the beam parameters during long pulses with a rather continuous release of caesium.

Figure 9 features photos of the SPIDER plasma driver plate showing evidence of BSI+ footprints: SPIDER has been operated with a PG mask covering most of the beamlet apertures, leaving only 28 open apertures out of a total of 1280. The central scheme shown in Figure 9 highlights the 28 open beamlets with filled circles; of these apertures, only the ones intercepting the plasma driver plate are actually identifiable on the plasma driver plate. Understanding the origin of these ions might yield useful information for the future SPIDER operation. During the recent operations a strong interaction with the EG occurred, with evidences of Cs removal from the EG surface (which would mostly occur as Cs+) and of Cu sputtering (which is considered to have only a rather mild probability of being sputtered]); however, only BSI+ originated from beam-gas interaction are relevant for future long-pulse operation, because the beam will operate at perveance match and no beam interaction with the grids shall occur. Correlating the BSI+ footprint positions with origin and mass of the ions was possible considering the expected trajectories inside the accelerator as discussed in the following.

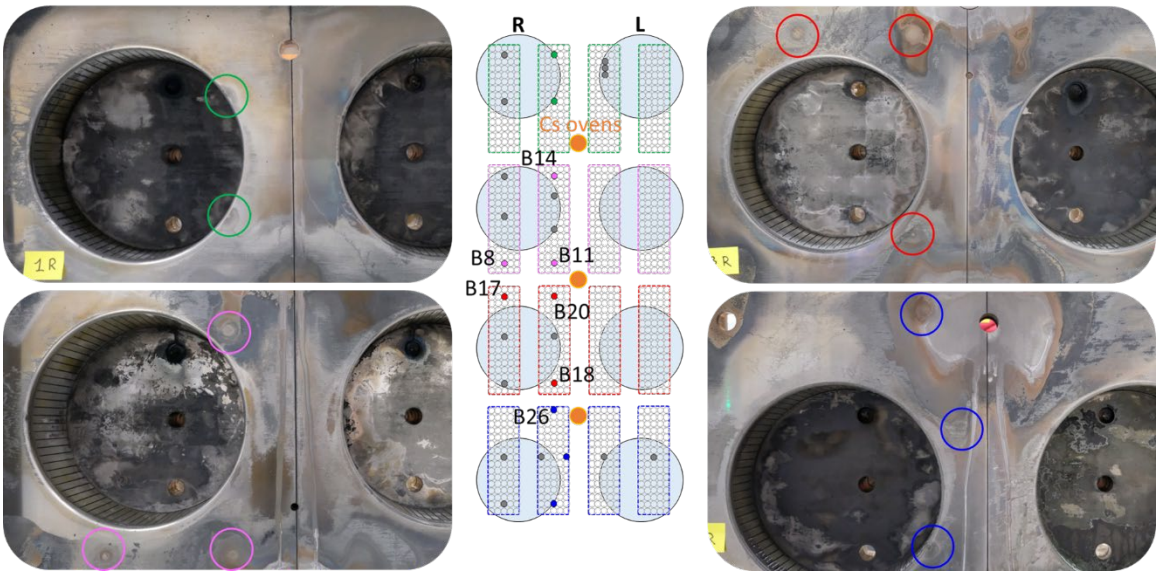


Figure 9 Photos of the plasma driver plate (PDP); the BSI footprints are highlighted with coloured circles. The central scheme represents the position of the beamlet apertures with respect to the drivers, with the filled circles representing the 28 apertures left open by the PG mask. Of the filled apertures, only the coloured ones are actually visible on the PDP surface. Some of the labelled BSI footprints were also characterised by chemical sampling.

When comparing the footprints of beamlets B8*-B17, B14*-B11* and B20-B18, a horizontal displacement can be estimated between the centroids of each pair, being roughly 3.5 mm, 3.3 mm and 5.8 mm respectively (the * mark labels beamlets of the 2nd segment from the top). This deflection can be related to the magnetic field inside the accelerator, generated by permanent magnets embedded in the EG, and magnets in all segments of the GG but the 2nd one [21]. As sketched in Figure 10, the orientation of the EG and GG magnets is opposite and, in both cases, it is alternated when moving along the vertical direction *y*, so that the sign of the vertical component of the field changes for each beamlet row. As a consequence, the backstreaming ion trajectories are deflected along the horizontal direction *x* and the related footprints on the plasma driver plate are shifted with respect to the centre of the correspondent grid aperture. The horizontal shift $x - x_{center}$ of the BSI+ footprints is either positive or negative depending on the sign of the vertical component of the magnetic field.

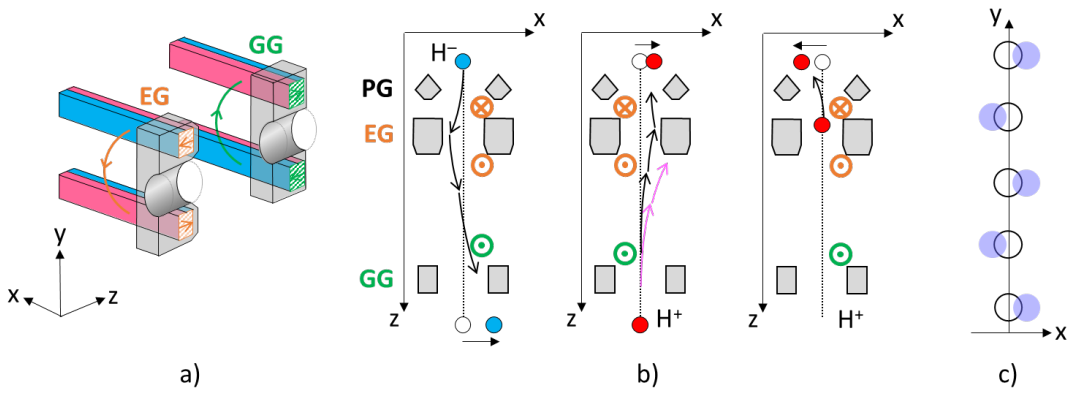


Figure 10 Simplified scheme of the permanent magnets embedded in the EG and GG grids (a), their effect on the beam ions and backstreaming ions trajectories assuming a paraxial approximation (b) and the resulting

displacement along the vertical direction (c). The second segment of the accelerator is not provided with permanent magnets embedded in the GG.

B14* and B11* are located in the second segment, so the shift can only be due to the EG magnets; as they belong to rows with opposite orientation of the EG permanent magnets, one can assume that two BSI footprints are shifted by the same quantity but in opposite directions: this implies that the actual deflection caused by the magnets is half of the measured misalignment, thus roughly 1.6 mm.

Considering a paraxial approximation of the BSI+ trajectories, a comparable value of the horizontal shift can be estimated by considering either $Cs^+$ or $Cu^+$ atoms coming from upstream the EG electrode with an energy of 2.5 keV and 8 keV respectively; these energies are compatible with the extraction voltage used during the most recent SPIDER operations[3]. A similar reasoning holds for the B8*-B17 beamlets, whereas for B20-B18 the horizontal shift is slightly larger but still compatible with $Cu^+$ ions born in front of the EG with 1.5-2 keV energy. This result could be explained as follows: for low extraction voltages, the poor beamlet optics can lead to the scraping of the inner surface of the EG apertures, which is made of copper, with the consequent formation of a certain fraction of Cu+ ions within the sputtered atoms. In addition, a more accurate investigation should be carried out for Cs+ ions generated by beam sputtering from the upstream side of the EG electrode (i.e. far from the beam axis, so that the paraxial approximation is no longer valid): the evidence of Cs removal from an annulus around the EG aperture is presented in Figure 6(b). We noted that the horizontal shift of the footprints shown in Figure 9 is always in the opposite direction with respect to the deflection of the related negative ion beamlet measured by the STRIKE calorimeter[22]; according to the calculation in paraxial approximation, this further suggests that the BSI+ are more likely generated upstream of the EG, as shown in Figure 10(b). However, it is also possible that the average trajectory of positive ions produced by ionization of the background gas between EG and GG crosses the EG aperture far from its axis, so that the paraxial approximation is no longer valid thus resulting in a deflection with opposite angle. A detailed investigation of BSI+ trajectories originated from the EG - GG gap and from the beam plasma in the transport region should use 3D numerical codes to consider non-zero effects of electrostatic lenses.

In the future operation without PG mask, the BSI will contribute to caesium release from the rear source walls, which in turn is transported towards the PG surface, enhancing the surface production of negative ions. In this case, BSI were observed to clean the surface from caesium. The results of the swab analyses, applied as described in the previous section, showed a clear removal of caesium in correspondence to the BSI footprint, with respect to the nearby area. Figure 11 shows caesium quantitative analyses obtained with ICP-MS on five different BSI footprints. To characterize the amount of caesium across each BSI footprint, 5 swabs (sampling points) were taken with uniform spacing.

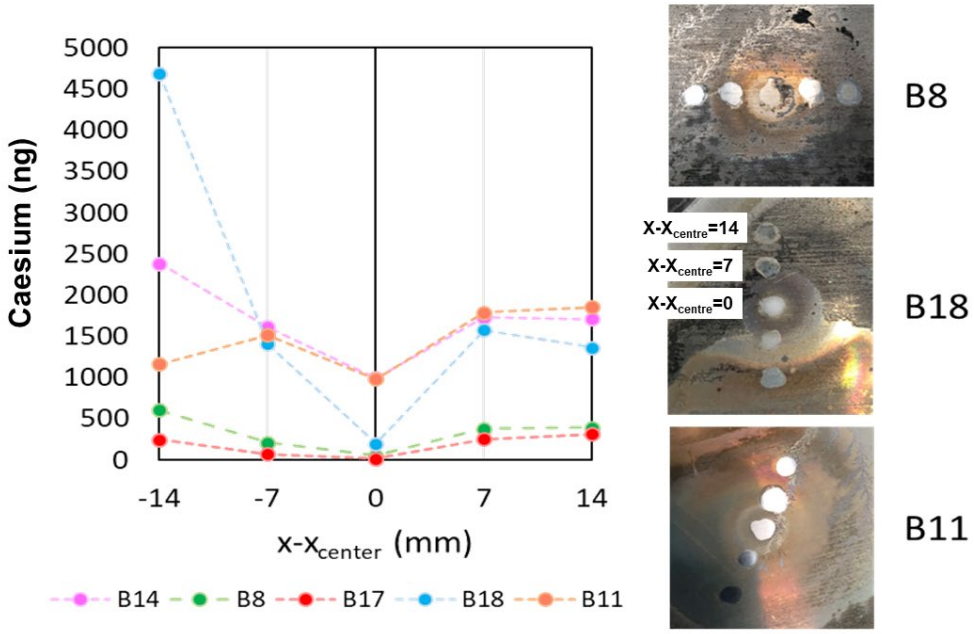


Figure 11 Plot of caesium concentration across BSI footprints. Photos show the swab sampling area and the effective cleaning procedure of a 5% $HNO_3$ solution

The caesium concentration for B8 and B17 is much lower with respect to other footprints, possibly because the former ones are further away from caesium ovens. The higher caesium concentration at x=-14 mm for B18 can be related to the shape of the stain surrounding the caesium oven close to the footprint (see Figure 8, top right).

At x=0 (i.e. at the centre of the BSI footprint) a clear reduction of caesium concentration was measured in all BSI footprints, see plot in Figure 11. This evidence can be related to the backstreaming positive ion current and caesium sputtering efficiency: in the following discussion, H+backstreaming ions coming from the beam plasma will be considered. Given a beamlet current and energy of 30 mA and $50\ keV$ (relevant to the final phase of the caesium campaign in SPIDER) and assuming a compensation degree $\psi = 3$ [23], the expected beam plasma density is of the order of $n_b = 2 \times 10^{15}\ \mathrm{m}^{-3}$. The backstreaming ion flux can be defined as $\Gamma_{BSI} = q n_b c_S$, with $c_S \approx 22\ \mathrm{km/s}$ being the Bohm velocity for an electron temperature of $5\ eV$. With a caesium sputtering yield of about 0.005[24], the caesium removal rate during the beam extraction phase is roughly $\Gamma_{rem} = 2.5 \times 10^{17}\ \mathrm{m^{-2}s^{-1}}$. Given a beam duty cycle of 15 s/4 min, at steady state (meaning that the same caesium amount removed by the BSI is re-deposited between the beam pulses), one can estimate a caesium deposition rate of the order of $\Gamma_{dep} = 1.5 \times 10^{16}\ \mathrm{m^{-2}s^{-1}}$. This result cannot be applied to B8 and B17 as almost all the caesium has been removed from the centre of the BSI footprint; for the region surrounding B11 and B14 instead, the caesium deposition rate can be estimated to be at least 2 or 3 times $\Gamma_{dep}$, as approximately 50% of caesium was removed from the footprint centre. Despite being a qualitative result, these estimations are useful for future SPIDER operations.

**Interaction of beam particles with surfaces**

Another evidence from beam particle interaction and secondary unwanted effects, inside the accelerator, was visible on the PG mask and around the PG apertures. As can be seen from Figure

12, these were covered by a layer of copper. The PG is molybdenum coated, so the copper layer could only be formed there by redeposition of neutral copper: this can be explained by the interaction of the beam particles with the inner surfaces of the EG apertures. Indeed, when the beamlet divergence is too large, the beam ions impact on the EG itself, sputtering copper atoms, which are then deposited backwards onto the downstream side of both the PG and the PG mask.

Figure 12 shows an example of the phenomenon, for which the beamlet clearance to the EG aperture becomes smaller and smaller up to a condition in which direct scraping occurs. In order to evaluate the importance of this phenomenon, simulation of the copper emission and deposition on surfaces was carried out using the view factor approach of the AVOCADO code [18]. Assuming a fraction of 30% of the beamlet current is intercepted, a sputtering yield of 0.009 for hydrogen considering the large incidence angle, and a beamlet current of 30 mA, the total emitted copper atoms would be $5x10^{14}$ 1/s from the cylindrical surface when the beamlet impinges on the EG aperture. With these parameters, the beamlet current and pulse duration can be compared to the profile of deposited copper on the downstream side of the PG, along a radial direction from the aperture, as presented in Figure 12(c). With the beamlet parameters considered here, a full layer of copper (roughly $5x10^{19}$ $m^{-2}$ for CFC lattice, 100 surface) would be obtained at s=3 mm, after 28 minutes beam-on time with such optics. This result is coherent with the beam-on duration and with the experimental evidence of the color of the copper deposition as a function of distance (see photos in Figure 12a).

In a large ion source, it is difficult to operate each single beamlet at perveance match, due to the non-uniformities in the available negative ion current from the plasma. In order to maximise the transmission of each beamlet in the accelerator, i.e. avoiding losses at the EG, the beamlet clearance shall be increased by enlarging the tapered part of the aperture, so that the extracted ions are less likely to interact with copper surfaces. The machining of the EG is now ongoing[25]. However, it is possible that the sputtering and redeposition of copper from the EG cannot be fully avoided during optics studies.

If copper re-deposition is not desired, it is possible to deposit molybdenum also on the EG. Yet, it is to be verified if covering with molybdenum the surface facing the plasma grid and the inner surface of the EG apertures would be enough to prevent sputtering by hydrogen at such large incidence angle. The minimum thickness needed for such molybdenum layer will also need to be estimated.

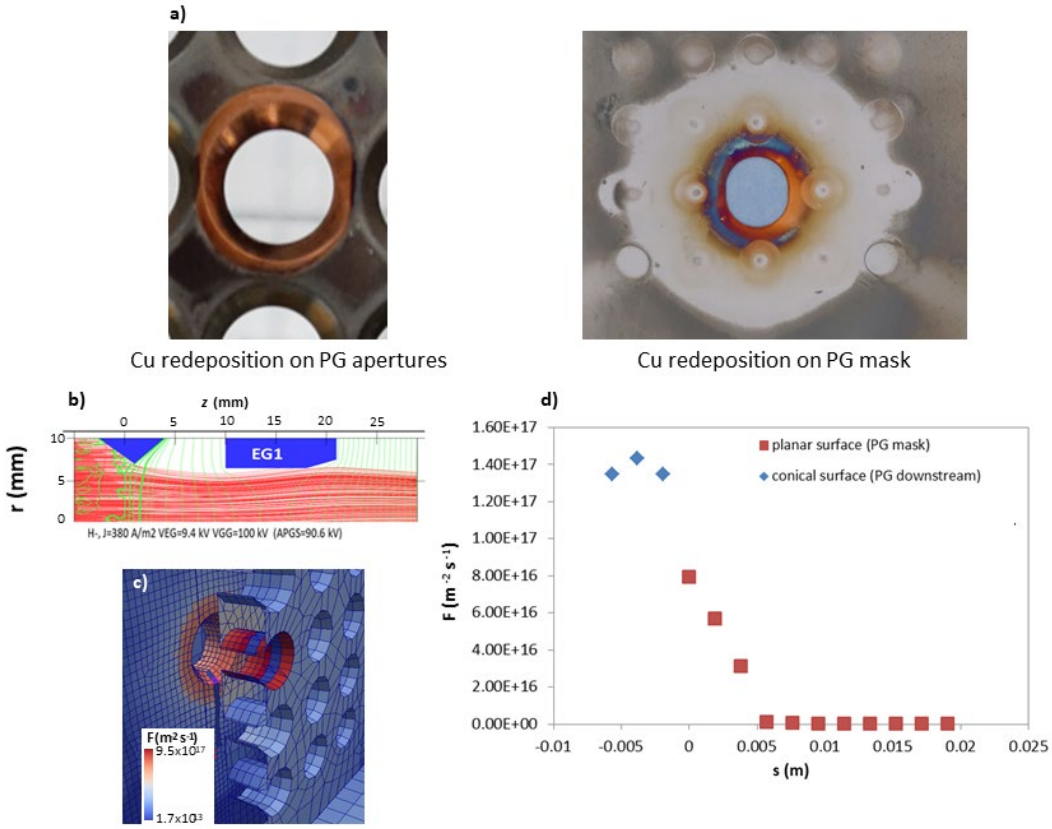


Figure 12 a) Photos of the PG apertures and PG mask covered by copper; b) ray tracing simulations of the beamlet optics, showing an overperveance condition in which the EG scrapes the beamlet; c) simulation of the copper atom emission (from the blue annulus inside the EG aperture) and deposition on the various surfaces of the accelerator electrodes, assuming an intercepted beamlet fraction of 30%, a sputtering yield of 0.009, and a sticking coefficient of 93% of copper atoms on surfaces; d) profile of copper atom deposition along the conical shape of the PG (blue points) and the PG mask (red points)

## 4 Conclusions and future work

SPIDER shutdown scheduled for end 2021-2022 for the refurbishment of major systems (namely the vacuum system, RF power generators and RF drivers and circuits on board the beam source) has been also exploited to improve the design or repair/refurbish components that have been unexpectedly damaged during operation. The main conclusions from the inspection of SPIDER beam source components are here summarised:

- The molybdenum coating was damaged during the first 3.5 years of SPIDER operation. SEM characterization on SPIDER molybdenum coating revealed a columnar morphology and cracks. An improved molybdenum coating is therefore required and an R&D campaign was launched to characterize SPIDER coating and improve its design for future operation.
- SEM analyses showed evidences of the non-homogeneous distribution of caesium in SPIDER beam source. *Post-mortem* analyses showed caesium to be distributed in the form of pits/stains. Caesium deposition will be characterized in the future by *in-situ* caesium deposition experiments (avoiding atmosphere/air exposure of caesiated samples), in a dedicated test bed[26].
- Uneven distribution of caesium in the beam source components in contact with the plasma was confirmed by modelling and experimental evidences (sampling and analyses

conducted by ICP-MS) on the EG and LW component. The uneven distribution was associated to the direct evaporation from caesium oven nozzle towards the EG; this information could be used to optimize caesium evaporation from the nozzles. The non-homogeneous distribution found over the LW is an indication of the caesium ionization in the plasma box, with the deposition in the form of $Cs^+$ at the magnetic cusps being dominant with respect to the neutral caesium deposited in between the cusps.

- Cleaning methods are being tested in SPIDER beam source components to identify the best method, while keeping in mind that cleaning of the ITER NBIs would have to be performed without disassembling the source. In the future, further caesium cleaning techniques will also be tested.
- BSIs footprints on the driver plate were characterised to understand the role of BSIs in removing caesium. Chemical analyses taken across BSI footprints have demonstrated the effective role of BSI in removing caesium
- Unwanted interaction of the beam particles with the EG apertures was confirmed: sputtered copper was found redeposited on the downstream side of both PG mask and PG apertures. This confirmed the interception of overperveance beamlets with the EG aperture; to enlarge the experimental window, allowing the beam transmission through the accelerator, the EG apertures will be reshaped with an enhanced tapering

## Acknowledgements

This work has been carried out within the framework of the ITER-RFX Neutral Beam Testing Facility (NBTF) Agreement and has received funding from the ITER Organization. The views and opinions expressed herein do not necessarily reflect those of the ITER Organization.
This work has also been carried out within the framework of the EUROfusion Consortium, funded by the European Union via the Euratom Research and Training Programme (Grant Agreement No 101052200 — EUROfusion). Views and opinions expressed are however those of the author(s) only and do not necessarily reflect those of the European Union or the European Commission. Neither the European Union nor the European Commission can be held responsible for them.
This work was supported in part by the Swiss National Science Foundation.

## References

[1] G. Serianni *et al.*, “SPIDER in the roadmap of the ITER neutral beams,” *Fusion Eng. Des.*, vol. 146, no. April, pp. 2539–2546, Sep. 2019.

[2] V. Toigo *et al.*, “On the road to ITER NBIs: SPIDER improvement after first operation and MITICA construction progress,” *Fusion Eng. Des.*, vol. 168, no. May, 2021.

[3] E. Sartori *et al.*, “First operations with caesium of the negative ion source SPIDER,” *Nucl. Fusion*, vol. 62, no. 8, p. 086022, Aug. 2022.

[4] G. Serianni *et al.*, “SPIDER, the Negative Ion Source Prototype for ITER: Overview of Operations and Cesium Injection,” *IEEE Trans. Plasma Sci.*, pp. 1–9, 2023.

[5] A. Maistrello, “Overview on electrical issues faced during the SPIDER experimental campaigns,” *under Rev.*, 2022.

[6] M. Siragusa *et al.*, “Conceptual design of scalable vacuum pump to validate sintered getter technology for future NBI application,” *Fusion Eng. Des.*, vol. 146, no. 633053,

pp. 87–90, 2019.

[7] G. Serianni *et al.*, “Spatially resolved diagnostics for optimization of large ion beam sources,” *Rev. Sci. Instrum.*, vol. 93, no. 8, p. 081101, Aug. 2022.

[8] ASTM D4453-17, “Standard practice for handling of high purity water samples,” 2017.

[9] C. Cavallini *et al.*, “Investigation of corrosion-erosion phenomena in the primary cooling system of SPIDER,” *Fusion Eng. Des.*, vol. 166, no. January, p. 112271, May 2021.

[10] C. Gasparrini *et al.*, “Water Degradation in ITER Neutral Beam Test Facility Cooling Circuits,” *IEEE Trans. Plasma Sci.*, pp. 1–5, 2022.

[11] C. Gasparrini *et al.*, “Water Chemistry in Fusion Cooling Systems: Borated Water for DTT Vacuum Vessel,” *IEEE Trans. Plasma Sci.*, pp. 1–5, 2022.

[12] S. Cristofaro, R. Friedl, and U. Fantz, “Correlation of Cs flux and work function of a converter surface during long plasma exposure for negative ion sources in view of ITER,” *Plasma Res. Express*, vol. 2, no. 3, p. 035009, Sep. 2020.

[13] A. Mimo, C. Wimmer, D. Wünderlich, M. Fröschle, and U. Fantz, “Towards the optimization of the Cs evaporation configuration for long pulse operation of negative ion sources,” *J. Phys. Conf. Ser.*, vol. 2244, no. 1, 2022.

[14] S. Cristofaro *et al.*, “Design and comparison of the Cs ovens for the test facilities ELISE and SPIDER,” *Rev. Sci. Instrum.*, vol. 90, no. 11, p. 113504, Nov. 2019.

[15] A. Rizzolo, M. Pavei, and N. Pomaro, “Caesium oven design and R&D for the SPIDER beam source,” *Fusion Eng. Des.*, vol. 88, no. 6–8, pp. 1007–1010, Oct. 2013.

[16] M. Spolaore, G. Serianni, A. Leorato, and F. D. Agostini, “Design of a system of electrostatic probes for the RF negative ion source of the SPIDER experiment,” *J. Phys. D. Appl. Phys.*, vol. 43, no. 12, p. 124018, Mar. 2010.

[17] V. Candela *et al.*, “Investigations on caesium dispersion and molybdenum coating on SPIDER components,” *Materials (Basel).*, vol. 16, no. 1, p. 206, Dec. 2022.

[18] E. Sartori and P. Veltri, “AVOCADO: A numerical code to calculate gas pressure distribution,” *Vacuum*, vol. 90, pp. 80–88, Apr. 2013.

[19] M. Barbisan, S. Cristofaro, L. Zampieri, R. Pasqualotto, and A. Rizzolo, “Laser absorption spectroscopy studies to characterize Cs oven performances for the negative ion source SPIDER,” *J. Instrum.*, vol. 14, no. 12, 2019.

[20] N. Marconato, E. Sartori, and G. Serianni, “Numerical and Experimental Assessment of the New Magnetic Field Configuration in SPIDER,” *IEEE Trans. Plasma Sci.*, vol. 50, no. 11, pp. 3884–3889, 2022.

[21] G. Chitarin, P. Agostinetti, D. Aprile, N. Marconato, and P. Veltri, “Improvements of the magnetic field design for SPIDER and MITICA negative ion beam sources,” *AIP Conf. Proc.*, vol. 040008, no. April 2015, 2015.

[22] A. Pimazzoni *et al.*, “Assessment of the SPIDER beam features by diagnostic calorimetry and thermography,” *Rev. Sci. Instrum.*, vol. 91, no. 3, 2020.

[23] E. Sartori, T. J. Maceina, P. Veltri, M. Cavenago, and G. Serianni, “Simulation of space charge compensation in a multibeamlet negative ion beam,” *Rev. Sci. Instrum.*, vol. 87, no. 2, p. 02B917, Feb. 2016.

[24] E. Sartori, S. Gorno, M. Fadone, and G. Serianni, “Analytical study of caesium-wall interaction parameters within a hydrogen plasma,” in *AIP Conference Proceedings*, 2018, vol. 2052, no. December, p. 020006.

[25] D. Marcuzzi *et al.*, “Lessons learned after three years of SPIDER operation and the first MITICA integrated tests,” *Fusion Eng. Des.*, vol. 191, no. February, p. 113590, Jun. 2023.

[26] A. Rizzolo *et al.*, “Characterization of the SPIDER Cs oven prototype in the CAesium Test Stand for the ITER HNB negative ion sources,” *Fusion Eng. Des.*, vol. 146, no. November 2018, pp. 676–679, 2019.